122nd ASEE Annual Conference & Exposition
June 14 - 17, 2015
Seattle, WA
Paper ID #12676

Projectile Motion with Aerodynamic Drag: The Cubic Law

Dr. Jeffrey C. Hayen, Oregon Institute of Technology

Jeffrey Hayen joined the faculty in the MMET Department at the Oregon Institute of Technology (OIT) in 2011. Before arriving at OIT, Jeffrey served as a Professor of Engineering, Mathematics, and Physics at Southwestern Oregon Community College for 16 years. Prior to that experience, he worked in the aerospace industry as a thermodynamicist and propellant analyst for high-performance upper-stage rockets at the Space Systems Division of the General Dynamics Corporation. He also has conducted research regarding structural dynamics and control for the Kajima Corporation of Japan, and he currently provides technical analyses and performs computational simulations for the United Launch Alliance in Denver. Jeffrey earned his B.S. and M.S. degrees in Mechanical Engineering from San Diego State University, and his Ph.D. degree in Applied Mechanics and Physics from the California Institute of Technology.

Projectile Motion with Aerodynamic Drag: The Cubic Law

Introduction

The effect of aerodynamic drag upon a projectile moving within a uniform gravitational field is routinely neglected in engineering mechanics and physics courses because of the mathematical complications that appear in the governing equations of motion when the drag effect is properly included. In contrast, this effect and its consequences are purposefully examined in this article. The drag force exerted on the projectile, as induced by its movement through the atmosphere, is modeled in accordance with a power-law relation that involves the projectile speed. But for the problem formulation chosen, the governing equations of motion are non-linear and coupled, yet they still permit an exact solution to be obtained in the form of a parametric description of the projectile motion (in the case of the *quadratic drag model*).

However, both the convenience and suitability of this form for pedagogical purposes are limited. Although it is exact, the solution consists of quadratures which cannot be analytically evaluated in terms of standard functions. This outcome has stimulated several investigators to pursue the development of approximate yet relatively accurate solutions for the motion of projectiles with the quadratic (i.e., second-degree) drag effect included [1,2].

When a projectile moves through a vacuum, it is well known that the trajectory corresponds to an inverted parabola, the graph of a quadratic polynomial. As will be explained, the trajectory that corresponds to the exact solution mentioned above has several properties also possessed by the graph of a cubic polynomial. Consequently, an approximation approach has emerged which is called the *cubic law*. This approach serves as the basis for the approximate solution presented herein. This approximate solution allows certain geometric characteristics associated with the trajectory to be revealed, as well as estimates for other quantities of interest to be obtained, for projectile motion in a resistant medium.

At the outset of this article, it should be disclosed that the content presented is not intended for a direct transference to students. Rather, a detailed exposition of the underlying steps that lead up to the primary results is provided for the benefit of educators, so that they may decide about the extent to which the material is conveyed to their students. The development of the exact solution is utilized to motivate and support the choice of the approximate solution form presented herein, and to supply exact results against which the approximate results can be compared. Ultimately, it is the sincere desire of the author to offer sufficient resource material so that the instructors who eventually adopt this material can adapt it to best fit their particular courses involving students at the freshman, sophomore, junior, or senior levels of study.

Problem Formulation

Projectile Motion Model Assumptions:

- The projectile is treated as a particle of mass m, and the resistant medium is quiescent.
- Any phenomena possibly depending upon the rotational dynamics or material extent of the projectile (e.g., gyroscopic, Bernoulli, or buoyancy effects) are neglected.
- A uniform gravitational field is omnipresent, characterized by the constant g.
- A power-law relation governs the drag force, characterized by the constants k and n.

Under these conditions, the vector-valued equation of motion for the projectile is given by

$$m\,\frac{d\mathbf{v}}{dt} = \mathbf{F}_{\mathrm{d}} + \mathbf{F}_{\mathrm{g}} \tag{1}$$

where

$$\mathbf{F}_{\mathrm{d}} \equiv -k\,v^{n-1}\,\mathbf{v} \quad , \quad \mathbf{F}_{\mathrm{g}} \equiv -m\,g\,\mathbf{j} \tag{2}$$

A graphical depiction of the projectile trajectory with the geometric configuration of the velocity vector $\mathbf{v}$ and the local path angle φ at a representative instant in time is provided in Fig. 1. The elapsed time of the projectile motion, as measured from the projection instant, is denoted by t. A free-body diagram indicating the forces acting on the projectile is also displayed in Fig. 1.

Next, it is useful to introduce the tangential and normal basis vectors $\mathbf{T}$ and $\mathbf{N}$, respectively:

$$\begin{aligned} &\mathbf{v} = v\,\mathbf{T} \quad ; \quad \mathbf{T}(\varphi) = \cos\varphi\,\mathbf{i} + \sin\varphi\,\mathbf{j} \\ &\mathbf{N}(\varphi) \equiv \mathbf{T}(\varphi + \tfrac{\pi}{2}) = -\sin\varphi\,\mathbf{i} + \cos\varphi\,\mathbf{j} \end{aligned} \tag{3}$$

Based upon Eqs. (2) and (3), the expressions on each side of Eq. (1) become

$$m\frac{d\mathbf{v}}{dt} = m\left[\frac{dv}{dt}\mathbf{T} + v\frac{d\mathbf{T}}{d\varphi}\frac{d\varphi}{dt}\right] = m\left[\frac{dv}{dt}\mathbf{T} + v\frac{d\varphi}{dt}\mathbf{N}\right] \tag{4}$$

$$\begin{aligned} \mathbf{F}_{\mathrm{d}} + \mathbf{F}_{\mathrm{g}} &= -k\,v^n\,\mathbf{T} - m\,g\left[(\mathbf{j}\cdot\mathbf{T})\,\mathbf{T} + (\mathbf{j}\cdot\mathbf{N})\,\mathbf{N}\right] \\ &= -(k\,v^n + m\,g\sin\varphi)\,\mathbf{T} - (m\,g\cos\varphi)\,\mathbf{N} \end{aligned} \tag{5}$$

Since these expressions must be equal, the corresponding scalar components yield

$$\begin{aligned} &\frac{dv}{dt} = -g\sin\varphi - \tfrac{k}{m}v^n \\ &v\frac{d\varphi}{dt} = -g\cos\varphi \end{aligned} \quad ; \quad \begin{aligned} &v(0) = v_{\mathrm{o}} \\ &\varphi(0) = \varphi_{\mathrm{o}} \end{aligned} \tag{6}$$

which is a set of coupled, non-linear, first-order ordinary differential equations (ODEs). Taken together with the initial conditions indicated for v and φ, these ODEs constitute an initial-value problem (IVP) involving a system of ODEs that collectively describe the projectile motion.

As is well known for the motion of a particle along a planar curve, the projectile speed v, local path angle φ, and position coordinates (x, y) are kinematically and geometrically related by

$$\begin{aligned} \frac{dx}{dt} &= v\cos\varphi \\ \frac{dy}{dt} &= v\sin\varphi \end{aligned} \quad ; \quad \begin{aligned} x(0) &= 0 \\ y(0) &= 0 \end{aligned} \tag{7}$$

where the origin O of the coordinate system adopted is assumed to coincide with the projection point. In summary, Eqs. (6) and (7) govern the motion and position of the projectile during the time interval $0 < t < t_i$, where t_i denotes the *impact instant* (at which $y = 0$ and $x > 0$).

In order to simplify the subsequent development, it is beneficial to transform these equations into non-dimensional forms by means of the following dimensionless-variable definitions:

$$\begin{aligned} \overline{v} &\equiv \frac{v}{v_o} \\ \overline{t} &\equiv \frac{g\,t}{v_o} \end{aligned} \quad , \quad \begin{aligned} \overline{x} &\equiv \frac{g\,x}{v_o^2} \\ \overline{y} &\equiv \frac{g\,y}{v_o^2} \end{aligned} \tag{8}$$

In the fields of engineering and physics, the utilization of dimensionless variables and groups of parameters can be very important, so this problem offers a context for undergraduate students in which the introduction of these concepts may occur. As a result, Eqs. (6) and (7) then become

$$\begin{aligned} \frac{d\overline{v}}{d\overline{t}} &= -\sin\varphi - \alpha^n\,\overline{v}^n \\ \overline{v}\,\frac{d\varphi}{d\overline{t}} &= -\cos\varphi \end{aligned} \quad ; \quad \begin{aligned} \overline{v}(0) &= 1 \\ \varphi(0) &= \varphi_o \end{aligned} \tag{9}$$

along with

$$\begin{aligned} \frac{d\bar{x}}{d\bar{t}} &= \bar{v}\cos\varphi \\ \frac{d\bar{y}}{d\bar{t}} &= \bar{v}\sin\varphi \end{aligned} \quad ; \quad \begin{aligned} \bar{x}(0) &= 0 \\ \bar{y}(0) &= 0 \end{aligned} \tag{10}$$

where $\alpha \equiv \left(\frac{k v_o^n}{m g}\right)^{1/n}$, which is a measure of the relative drag effect. It is a dimensionless group of parameters, and it will be called the *medium resistance intensity*.

It is advantageous to merge the ODEs indicated in Eqs. (9) in order to eliminate the variable $\bar{t}$. Based upon the differential relation $d\bar{v}/d\bar{t} = (d\bar{v}/d\varphi)(d\varphi/d\bar{t})$, these ODEs can be combined to obtain a single master equation of motion:

$$\frac{d\bar{v}}{d\varphi}\cos\varphi = \bar{v}\sin\varphi + \alpha^n \bar{v}^{n+1} \quad ; \quad \begin{aligned} \bar{v}(0) &= 1 \\ \varphi(0) &= \varphi_o \end{aligned} \tag{11}$$

Two cases of this equation are considered below, but only one case is significantly explored.

Exact Solution: The Linear Drag Model $\Rightarrow$ $n = 1$, $\alpha \equiv \frac{k v_o}{m g}$

In this case, with $0 < \varphi_o < \frac{\pi}{2}$, Eqs. (11) become

$$\frac{d\bar{v}}{d\varphi}\cos\varphi = \bar{v}\sin\varphi + \alpha \bar{v}^2 \quad ; \quad \begin{aligned} \bar{v}(0) &= 1 \\ \varphi(0) &= \varphi_o \end{aligned} \tag{12}$$

which is known as a *Bernoulli differential equation.* Employing methods typically covered in a sophomore or junior-level differential equations course [3], it can be shown that the solution of this equation yields

$$\bar{v} = \frac{\cos\varphi_o \sec\varphi}{1 + \alpha\cos\varphi_o\,(\tan\varphi_o - \tan\varphi)} \tag{13}$$

After re-combining this result with Eqs. (9) and again utilizing $d\bar{v}/d\bar{t} = (d\bar{v}/d\varphi)(d\varphi/d\bar{t})$, it can be determined (and is a worthwhile exercise to show) that

$$\begin{aligned} \bar{v} &= \sqrt{(\cos\varphi_o)^2 + \left[\sin\varphi_o + \tfrac{1}{\alpha}(1 - e^{\alpha\bar{t}})\right]^2}\; e^{-\alpha\bar{t}} \\ \varphi &= \tan^{-1}\left\{\tan\varphi_o + \tfrac{1}{\alpha}\sec\varphi_o\,(1 - e^{\alpha\bar{t}})\right\} \end{aligned} \tag{14}$$

Apparently, these specific results, expressing the variation of $\bar{v}$ and φ with $\bar{t}$, are original and not found elsewhere in the literature. Finally, Eqs. (14) can be utilized with Eqs. (10) to obtain

$$\begin{aligned} \bar{x} &= \left[\tfrac{1}{\alpha}\cos\varphi_o\right](1 - e^{-\alpha\bar{t}}) \\ \bar{y} &= \left[\tfrac{1}{\alpha}\sin\varphi_o + (\tfrac{1}{\alpha})^2\right](1 - e^{-\alpha\bar{t}}) - \tfrac{1}{\alpha}\bar{t} \end{aligned} \tag{15}$$

which represents an *exact time-explicit solution* for this model of the problem. This solution for $\bar{x}$ and $\bar{y}$ has previously appeared (in an alternative form) in the literature [4].

For projectile motion applications, the linear drag model is not especially accurate for reasons to be explained. Nevertheless, these results are offered for educational purposes and enrichment, since the mathematics involved is less formidable than for the next case, and they certainly are more realistic in comparison to results obtained when aerodynamic drag is altogether ignored (i.e., the traditional solution for projectile motion in a vacuum). Also, it is quite possible that for introductory physics and engineering mechanics courses, the expressions given in Eqs. (14) and (15) are entirely satisfactory as a first effort to account for the drag effect in projectile motion.

Exact Solution: The Quadratic Drag Model $\Rightarrow$ $n = 2$, $\alpha \equiv \sqrt{\frac{k v_o^2}{m g}}$

In this case, with $0 < \varphi_o < \frac{\pi}{2}$, Eqs. (11) become

$$\frac{d\overline{v}}{d\varphi}\cos\varphi = \overline{v}\sin\varphi + \alpha^2\,\overline{v}^3 \quad ; \quad \begin{matrix}\overline{v}(0)=1\\ \varphi(0)=\varphi_o\end{matrix} \tag{16}$$

or, equivalently,

$$\frac{d\overline{v}}{d\varphi} - (\tan\varphi)\,\overline{v} = \alpha^2\,(\sec\varphi)\,\overline{v}^3 \quad ; \quad \begin{matrix}\overline{v}(0)=1\\ \varphi(0)=\varphi_o\end{matrix} \tag{17}$$

which is also a Bernoulli differential equation. Applying the same solution method [3] as above to this equation (actually, only part of the usual procedure is needed) yields

$$\frac{d}{d\varphi}\left[(\overline{v}\cos\varphi)^{-2}\right] = -2\,\alpha^2\,(\sec\varphi)^3 \tag{18}$$

Next, unlike the development in the case of the linear drag model, it is useful to transform this equation in terms of a new independent variable u in order to achieve further progress. u is the *opposite local path slope* (or, more simply, the *opposite slope*), defined as

$$u \equiv -\tan\varphi \tag{19}$$

Under this transformation, and with the aid of a few trigonometric identities, Eq. (18) yields

$$\frac{d}{du}\left[\frac{1+u^2}{\overline{v}^2}\right] = 2\,\alpha^2\sqrt{1+u^2} \tag{20}$$

which, when symbolically integrated, becomes

$$\int_{1+\xi_o^2}^{\frac{1+u^2}{\overline{v}^2}} dq = 2\,\alpha^2\int_{-\xi_o}^{u}\sqrt{1+p^2}\;dp \tag{21}$$

where $\xi_o \equiv \tan\varphi_o$ is the *projection slope*. For the initial conditions stated in Eqs. (16) and (17), observe that $\bar{v} = 1$ when $u = -\xi_o$, and also recognize that p and q are merely *dummy variables* of integration. After the indicated operations are performed, Eq. (21) yields

$$\bar{v} = \sqrt{\frac{1+u^2}{f(u;\xi_o)}} \tag{22}$$

where the function f arises from the integration process and is defined by

$$\begin{aligned} f(u;\xi_o) &\equiv \alpha^2\left[r(u) + r(\xi_o)\right] + (1+\xi_o^2) \\ r(u) &\equiv u\sqrt{1+u^2} + \sinh^{-1}(u) \end{aligned} \tag{23}$$

The entire projectile trajectory is described by $-\xi_o \le u \le \xi_i$, where $\xi_i \equiv \tan\left|\varphi_i\right|$ is the (absolute) *impact slope*, whose evaluation is discussed in a later section.

Based upon the previous expression for $d\bar{x}/d\bar{t}$ and the definition of u, observe that

$$\frac{d\bar{x}}{du}\frac{du}{d\varphi}\frac{d\varphi}{d\bar{t}} = \bar{v}\cos\varphi \quad \Rightarrow \quad \frac{d\bar{x}}{du} = \frac{\bar{v}^2}{1+u^2} \tag{24}$$

In a similar manner, expressions for $d\bar{y}/du$ and $d\bar{t}/du$ can be obtained, collectively yielding

$$\begin{aligned} \frac{d\bar{x}}{du} &= \frac{\bar{v}^2}{1+u^2} \\ \frac{d\bar{y}}{du} &= \frac{-u\,\bar{v}^2}{1+u^2} \end{aligned} \quad , \quad \frac{d\bar{t}}{du} = \frac{\bar{v}}{\sqrt{1+u^2}} \tag{25}$$

Equation (22) enables these equations to be symbolically integrated, and thereby obtain

$$\overline{x} = \int_{-\xi_o}^{u} \frac{dp}{f(p;\xi_o)} \qquad , \qquad \overline{t} = \int_{-\xi_o}^{u} \frac{dp}{\sqrt{f(p;\xi_o)}} \tag{26}$$
$$\overline{y} = \int_{-\xi_o}^{u} \frac{-\,p\,dp}{f(p;\xi_o)}$$

These relations offer a parametric description of the projectile motion in terms of the variable u; again, p is only a dummy variable of integration. In the general case with $\alpha > 0$, these integrals cannot be analytically evaluated in terms of standard functions but can be numerically evaluated. Thus, an *exact time-implicit solution* for this model of the problem has been obtained.

As a way of building confidence in the results obtained so far, suppose that $\alpha = 0$ (i.e., medium resistance is absent). Then $f(p;\xi_o) = 1 + \xi_o^2$ (a constant), in which case the integrals appearing in Eqs. (26) are easily and immediately evaluated to yield

$$\overline{x} = \frac{u + \xi_o}{1 + \xi_o^2} \qquad , \qquad \overline{t} = \frac{u + \xi_o}{\sqrt{1 + \xi_o^2}} \tag{27}$$
$$\overline{y} = \frac{\xi_o^2 - u^2}{2(1 + \xi_o^2)}$$

With the aid of a few trigonometric identities, the variable u then may be eliminated from these expressions (recall that $\xi_o \equiv \tan\varphi_o$ with $0 < \varphi_o < \frac{\pi}{2}$) to obtain

$$\begin{aligned} \overline{x} &= (\cos\varphi_o)\,\overline{t} \\ \overline{y} &= (\sin\varphi_o)\,\overline{t} - \tfrac{1}{2}\overline{t}^{\,2} \end{aligned} \quad \Rightarrow \quad \overline{y} = (\tan\varphi_o)\,\overline{x} - \tfrac{1}{2}(\sec\varphi_o)^2\,\overline{x}^{\,2} \tag{28}$$

which may be recognized as the results for projectile motion in a vacuum under the influence of a uniform gravitational field (expressed in terms of the dimensionless variables employed). With reference to Eqs. (8), these results can be recast in terms of regular variables to reveal their more familiar forms:

$$\begin{aligned} x &= (v_{\mathrm{o}} \cos\varphi_{\mathrm{o}})\, t \\ y &= (v_{\mathrm{o}} \sin\varphi_{\mathrm{o}})\, t - \tfrac{1}{2} g\, t^2 \end{aligned} \quad \Rightarrow \quad y = (\tan\varphi_{\mathrm{o}})\, x - \frac{g}{2 v_{\mathrm{o}}^2} (\sec\varphi_{\mathrm{o}})^2\, x^2 \tag{29}$$

Remark: Based upon fluid mechanics principles, it can be demonstrated that a drag force model whose force magnitude is proportional to the projectile-speed squared yields greater accuracy for the predicted motion of a projectile when compared to its actual motion in a resistant medium [5,6]. Accordingly, the quadratic drag model is solely utilized for the remainder of this article.

Approximate Solution: The Cubic Law

Although the integrals in Eqs. (26) cannot be analytically evaluated, it is still possible to deduce important properties of the exact trajectory from these expressions without actually numerically evaluating these integrals. These properties validate the choice of a certain function that provides the basis for an approximate solution for projectile motion in a resistant medium.

In a more detailed treatment of this problem, it can be shown [7] that every trajectory for $\alpha > 0$ must be asymmetric about a vertical axis through the apex, as is depicted in Fig. 2, where $\xi_{\mathrm{a}}(\bar{y})$ and $\xi_{\mathrm{d}}(\bar{y})$ respectively denote the *absolute slopes* of the trajectory at arbitrary points A and D with a common elevation $\bar{y}$ on the ascent and descent branches. Specifically, $\xi_{\mathrm{a}}(\bar{y}) < \xi_{\mathrm{d}}(\bar{y})$ for $0 \le \bar{y} < \bar{A}$, where $\bar{A}$ denotes the *altitude* of the apex, which is the maximum elevation attained by the projectile as it moves along the trajectory.

Fortuitously, it can be shown [8] that the graph of a cubic polynomial possesses this property as well, since this curve typically has an asymmetric arched segment. In stark contrast, the graph of a quadratic polynomial (i.e., an inverted parabola) does not possess this property.

Accordingly, consider a cubic polynomial that expresses $\bar{y}$ in terms of $\bar{x}$ with the form

$$\overline{y} = -\overline{a}\,\overline{x}^3 - \overline{b}\,\overline{x}^2 + \overline{c}\,\overline{x} \tag{30}$$

where $\overline{a}$, $\overline{b}$, and $\overline{c}$ are presumed to be positive constants. This particular equation, referred to as the *cubic law*, is selected because its graph has the following additional properties, beyond the property described above, which qualify it to be a suitable approximation for an actual trajectory of a projectile:

1. The graph has an intercept at the origin (corresponding to the projection point).

2. The graph has a relative maximum (i.e., an apex for the projectile trajectory) at

$$\overline{x} = \frac{\sqrt{\overline{b}^2 + 3\overline{a}\,\overline{c}} - \overline{b}}{3\overline{a}} \tag{31}$$

which lies to the *right of the origin* (consistent with the direction of projectile motion).

3. The graph has an inflection point at

$$\overline{x} = \frac{-\overline{b}}{3\overline{a}} \tag{32}$$

which lies to the *left of the origin*. Thus: (a) the graph is concave downward for $\overline{x} \geq 0$ because $-\overline{a} < 0$; and (b) the inflection point is not included on the arched segment of the curve which is utilized to model the projectile trajectory, since an actual trajectory would lack such a feature.

Based upon typical values for the polynomial coefficients, a representative graph of Eq. (30) is displayed in Fig. 3. Observe that only the segment of the curve within Quadrant I is appropriate and useful for modeling a projectile trajectory.

Since $u \equiv -\tan\varphi$ and $\tan\varphi = d\bar{y}/d\bar{x}$ via Eqs. (10), differentiation of Eq. (30) reveals that

$$u = 3\bar{a}\,\bar{x}^2 + 2\bar{b}\,\bar{x} - \bar{c} \tag{33}$$

which can be solved for $\bar{x}$ (with $\bar{x} \geq 0$) in terms of u to obtain

$$\bar{x} = \frac{\sqrt{\bar{b}^2 + 3\bar{a}\,(u + \bar{c})} - \bar{b}}{3\bar{a}} \tag{34}$$

Then, implicit differentiation of this relation yields an expression for $du/d\bar{x}$:

$$\frac{du_{\mathrm{A}}}{d\bar{x}} = g(u;\xi_{\mathrm{o}}) \quad ; \quad g(u;\xi_{\mathrm{o}}) = 2\sqrt{\bar{b}^2 + 3\bar{a}\,(u + \bar{c})} \tag{35}$$

where the subscripts A and E will respectively identify results based upon the approximate and exact solutions. The expressions for the coefficients $\bar{a}$, $\bar{b}$, and $\bar{c}$ are yet to be determined, but it will be shown that they all depend upon ξ_{o} ($\bar{a}$ also depends upon α).

Compare this result with the expression for $du/d\bar{x}$ obtained by means of the exact solution:

$$\frac{du_{\mathrm{E}}}{d\bar{x}} = f(u;\xi_{\mathrm{o}}) \quad ; \quad f(u;\xi_{\mathrm{o}}) \equiv \alpha^2\,[r(u) + r(\xi_{\mathrm{o}})] + (1 + \xi_{\mathrm{o}}^2) \tag{36}$$

which is obtained from Eqs. (22) and (24).

Based upon this comparison, it is quite natural to interpret the function g as an approximation to the function f, in which case it may be inferred from Eqs. (26) that

$$\overline{x} = \int_{-\xi_o}^{u} \frac{dp}{g(p;\xi_o)} \quad , \quad \overline{t} = \int_{-\xi_o}^{u} \frac{dp}{\sqrt{g(p;\xi_o)}} \qquad (37)$$
$$\overline{y} = \int_{-\xi_o}^{u} \frac{-\,p\,dp}{g(p;\xi_o)}$$

in an approximate sense. After substitution for g with the expression obtained above, but with $\overline{c} = \xi_o$ (this assignment will be satisfactorily justified below), it is found that these integrals can be analytically evaluated to yield the purely algebraic results

$$\overline{x} = \frac{u + \xi_o}{\sqrt{\overline{b}^2 + 3\overline{a}\,(u + \xi_o)} + \overline{b}}$$
$$\overline{y} = \frac{(u + \xi_o)\left[(2\,\xi_o - u)\sqrt{\overline{b}^2 + 3\overline{a}\,(u + \xi_o)} + (\xi_o - 2u)\,\overline{b}\right]}{3\left[\sqrt{\overline{b}^2 + 3\overline{a}\,(u + \xi_o)} + \overline{b}\right]^2} \qquad (38)$$

along with

$$\overline{t} = \frac{2\sqrt{2}\,(u + \xi_o)\left[\overline{b}^4 + 3\overline{a}\,\overline{b}^2\,(u + \xi_o) + 3\overline{a}^2\,(u + \xi_o)^2\right]}{\left\{\left[\overline{b}^2 + 3\overline{a}\,(u + \xi_o)\right]^{3/4} + \overline{b}^{3/2}\right\}\left\{\left[\overline{b}^2 + 3\overline{a}\,(u + \xi_o)\right]^{3/2} + \overline{b}^3\right\}} \qquad (39)$$

Thus, an *approximate time-implicit solution* for this model of the problem has been obtained. It is valid over the opposite-slope interval $-\xi_o \le u \le \xi_i$, for which $\xi_i = u\,\big|_{\overline{y}=0 \text{ and } \overline{x}>0}$.

Although Eqs. (38) and (39) enable (in principle) the position of the projectile to be determined as a function of the elapsed time, the trajectory is established by Eq. (30) alone. In fact, Eq. (30) is almost exclusively utilized to obtain the remaining results developed below.

Determination of the Cubic Law Coefficients

The approximate solution cannot be utilized for practical purposes until the values of $\overline{a}$, $\overline{b}$, and

$\bar{c}$ have been determined. It is possible to conceive of several approaches to the determination of these coefficients [8]. The approach adopted below causes the approximate trajectory to match signature geometric characteristics of the exact trajectory, but without the need to perform any numerical integration. Accordingly, it is required that

$$u_{\mathrm{A}} = u_{\mathrm{E}} = -\xi_{\mathrm{o}} \quad \text{at} \quad \bar{x} = 0 \tag{40}$$

(i.e., *matched slope* of the trajectories at the origin) along with

$$g(u;\xi_{\mathrm{o}}) = f(u;\xi_{\mathrm{o}}) \quad \text{at} \quad \begin{cases} u = -\xi_{\mathrm{o}} \\ u = 0 \end{cases} \tag{41}$$

(i.e., *matched curvature* of the trajectories at, separately, the origin and the apex; recall that the functions f and g each provide $du/d\bar{x}$ for their respective trajectories). Enforcement of these conditions via Eqs. (33), (35), and (36) yields the required polynomial coefficients:

$$\bar{a} = \frac{\alpha^2 r(\xi_{\mathrm{o}})}{6\xi_{\mathrm{o}}}\left[\frac{\alpha^2 r(\xi_{\mathrm{o}})}{2} + (1+\xi_{\mathrm{o}}^2)\right] \quad , \quad \begin{matrix} \bar{b} = \dfrac{1+\xi_{\mathrm{o}}^2}{2} \\ \bar{c} = \xi_{\mathrm{o}} \end{matrix} \tag{42}$$

By means of Eqs. (8), Eq. (30) may be recast in terms of regular variables to obtain

$$y = -a\,x^3 - b\,x^2 + c\,x \tag{43}$$

for which

$$a = \left[\frac{g}{v_{\mathrm{o}}^2}\right]^2 \frac{\alpha^2 r(\xi_{\mathrm{o}})}{6\xi_{\mathrm{o}}}\left[\frac{\alpha^2 r(\xi_{\mathrm{o}})}{2} + (1+\xi_{\mathrm{o}}^2)\right] \quad , \quad \begin{matrix} b = \left[\dfrac{g}{v_{\mathrm{o}}^2}\right]\left[\dfrac{1+\xi_{\mathrm{o}}^2}{2}\right] \\ c = \xi_{\mathrm{o}} \end{matrix} \tag{44}$$

An intriguing characteristic of the approximate solution for projectile motion with aerodynamic drag included is that it has the same form as the exact solution for projectile motion in a vacuum, as confirmed by Eqs. (29), with $\xi_o \equiv \tan\varphi_o$, except for the addition of a single cubic term whose coefficient is a. *This fact renders the cubic law as a simple extension of the traditional result*.

Some sample trajectories are displayed in Figs. 4 and 5 for (respectively) $\varphi_o = 45^\circ$ and 60°. The trajectory cases correspond to $\alpha = 1.5,\ 1.0,\ 0.5,$ and 0.0 in each figure. Also, $v_o = 10\ \text{m/s}$ and $g = 9.81\ \text{m/s}^2$ were utilized to generate these particular results. These figures were created with the chart-production capabilities available within an EXCEL® workbook. The solid and dashed curves identify results generated with the approximate and exact solutions (respectively), but it was not possible to obtain experimental results for a comparison with the exact and approximate results, given the limitations imposed for the completion of this article.

For this selection of values for α, it seems evident that the approximate solution is reasonably accurate. However, in order to address the question of what values for α might be encountered in applications of projectile motion, a situation very familiar to most readers is considered in the Appendix to this article, and it reveals what could be regarded as a typical value for α.

Maximum Projectile Range: Exact Analysis

In applications of projectile motion, the maximum projectile range and optimal projection angle are of considerable interest. As expected, the *projectile range* $\bar{R}$ is defined as the value of $\bar{x}$ at the impact point. As a result, $\bar{y} = 0$ at $\bar{x} = \bar{R}$ (with $\bar{R} > 0$).

In order to maximize $\bar{R}$, ξ_o must be optimized, but subject to the condition $\bar{y} = 0$ at $\bar{x} = \bar{R}$. As a result, based upon the expressions obtained for $\bar{x}$ and $\bar{y}$, ξ_i must be optimized as well. Thus, a *constrained optimization problem* can be formulated as follows:

$$\begin{aligned} &\text{Optimization Target:} \quad \bar{R}(\xi_o, \xi_i) \\ &\text{Constraint Relation:} \quad G(\xi_o, \xi_i) = 0 \end{aligned} \tag{45}$$

where

$$\begin{aligned} \bar{R}(\xi_o, \xi_i) &\equiv \bar{x}\,\big|_{u=\xi_i} = \int_{-\xi_o}^{\xi_i} \frac{dp}{f(p, \xi_o)} \\ G(\xi_o, \xi_i) &\equiv \bar{y}\,\big|_{u=\xi_i} = \int_{-\xi_o}^{\xi_i} \frac{-p\,dp}{f(p, \xi_o)} \end{aligned} \tag{46}$$

This optimization problem may be solved by the *method of Lagrange multipliers* [9], but such an effort is beyond the scope of this article. The values of ξ_o^* and ξ_i^* required to satisfy Eqs. (45) and (46) have been numerically determined [7] for various values of α. With these values, the maximum range $\bar{R}^*$ can be evaluated via the relation for $\bar{R}(\xi_o, \xi_i)$ in Eqs. (46). These results are utilized in the next section to assess/judge the accuracy of the analogous results generated via the cubic law.

Maximum Projectile Range: Approximate Analysis

As described above, $\bar{y} = 0$ at $\bar{x} = \bar{R}$ (with $\bar{R} > 0$). The cubic law, Eq. (30), then requires that

$$\bar{a}\,\bar{R}^2 + \bar{b}\,\bar{R} - \xi_o = 0 \tag{47}$$

where the expressions for $\bar{a}$ and $\bar{b}$ were previously determined but are temporarily suppressed in order to simplify the notation. The positive solution to this equation is given by

$$\bar{R} = \frac{\sqrt{\bar{b}^2 + 4\bar{a}\,\xi_o} - \bar{b}}{2\bar{a}} = \frac{2\xi_o}{\sqrt{\bar{b}^2 + 4\bar{a}\,\xi_o} + \bar{b}} \tag{48}$$

Although approximate, this expression can be utilized to accurately estimate the maximum value of $\bar{R}$ (denoted by $\bar{R}^*$) and the optimal value of ξ_o that produces $\bar{R}^*$ (denoted by ξ_o^*) for each value of α considered. The necessary condition for optimality is $d\bar{R}/d\xi_o = 0$. After Eq. (47) is implicitly differentiated with respect to ξ_o and the condition $d\bar{R}/d\xi_o = 0$ is applied to this result, it is found that

$$\frac{d\bar{a}}{d\xi_o}\bar{R}^2 + \frac{d\bar{b}}{d\xi_o}\bar{R} - 1 = 0 \tag{49}$$

for which, from Eqs. (42),

$$\begin{aligned} \frac{d\bar{a}}{d\xi_o} &= \frac{\alpha^2}{6\xi_o^2}\left\{\left[\alpha^2 r(\xi_o) + (1+\xi_o^2)\right]\xi_o r'(\xi_o) - \left[\tfrac{1}{2}\alpha^2 r(\xi_o) + (1-\xi_o^2)\right] r(\xi_o)\right\} \\ \frac{d\bar{b}}{d\xi_o} &= \xi_o \end{aligned} \tag{50}$$

where $r'(u) = 2\sqrt{1+u^2}$. Equation (49) provides a relation between ξ_o^* and α since $\bar{a}$, $\bar{b}$, and $\bar{R}$ have been previously expressed in terms of ξ_o ($\bar{a}$ and $d\bar{a}/d\xi_o$ also depend upon α). For each α considered, the value of ξ_o^* required by this equation was then numerically determined. Each ξ_o^* then yields a value of $\bar{R}^*$ via Eq. (48). By this procedure, the results displayed in Figs. 6, 7, and 8 were generated ($\varphi_o^* = \tan^{-1}(\xi_o^*)$ and $\left|\varphi_i^*\right| = \tan^{-1}(\xi_i^*)$). Again, the solid and dashed curves identify results for the approximate and exact solutions (respectively). The presence of ξ_i^* and φ_i^* in these figures is clarified in the next section. Observe that $\varphi_o^* < 45^\circ$ if $\alpha > 0$, and that φ_o^* appears to be a strictly-decreasing function of α, which usually initiates an interesting discussion with students when attempting to explain this physical feature.

Further Estimates by the Approximate Solution

The approximate solution can be exploited to estimate other quantities of interest related to the

projectile motion without the difficulties associated with directly utilizing the exact solution (i.e., the numerical evaluation of several integrals).

Observe that $\bar{y} = \bar{A}$ when $u = 0$ ($\bar{A}$ is the *altitude* of the trajectory apex), in which case the last relation in Eqs. (38) reveals that

$$\bar{A} = \frac{\xi_o^2 \left[2\sqrt{\bar{b}^2 + 3\bar{a}\,\xi_o} + \bar{b} \right]}{3\left[\sqrt{\bar{b}^2 + 3\bar{a}\,\xi_o} + \bar{b} \right]^2} \tag{51}$$

Observe that $\bar{t} = \bar{t}_a$ when $u = 0$ ($\bar{t}_a$ is the *ascent time*, the elapsed time needed for the projectile to reach the trajectory apex), in which case Eq. (39) reveals that

$$\bar{t}_a = \frac{2\sqrt{2}\,\xi_o \left[\bar{b}^4 + 3\bar{a}\,\bar{b}^2\,\xi_o + 3\bar{a}^2\,\xi_o^2 \right]}{\left\{ \left[\bar{b}^2 + 3\bar{a}\,\xi_o \right]^{3/4} + \bar{b}^{3/2} \right\} \left\{ \left[\bar{b}^2 + 3\bar{a}\,\xi_o \right]^{3/2} + \bar{b}^3 \right\}} \tag{52}$$

Recall that $u = \xi_i$ when $\bar{x} = \bar{R}$ (ξ_i is the *impact slope*), in which case Eq. (33) becomes

$$\xi_i = 3\bar{a}\,\bar{R}^2 + 2\bar{b}\,\bar{R} - \xi_o \tag{53}$$

Although Eq. (53) may be applied to any trajectory, suppose that it is evaluated with ξ_o^* and $\bar{R}^*$ for a given α. Then it provides the value of ξ_i^* for an optimal trajectory case. It is this result that appears along with ξ_o^* in Fig. 6. The deviation between the exact and estimated values for ξ_i^* can be attributed to the fact that the requirements stipulated in Eqs. (40) and (41) target the ascent branch of the projectile trajectory, so the accuracy of the approximate solution is expected to diminish along the descent branch. However, as can be seen from Figs. 7 and 8, the accuracy of the estimated values for φ_o^* and $\bar{R}^*$ are quite excellent in comparison to their exact values. It is this outcome that undeniably confirms the overall success of the cubic law.

Conclusion

In this article, an exact solution for projectile motion with aerodynamic drag included was first developed and presented. This approach was selected for two reasons: to (1) reveal properties that motivate and support the choice of an analytically amenable function that serves as the basis of an approximate solution; and (2) provide exact results against which the approximate results can be compared. However, the most important outcomes of the efforts represented herein are the estimates and insights obtained by means of the approximate solution (i.e., the cubic law). It is these results that enable this more realistic version of the classic projectile motion problem to be more accessible to and better understood by students in physics and engineering — in a way that a numerical treatment alone of the governing equations could not easily reveal.

The quadratic drag model played the central role in this article because it is widely regarded (as established by experiments) to be more accurate than the linear drag model. But, as previously mentioned, it may be that the results obtained from the linear drag model are more appropriate for students at lower-division levels. However, utilization of the trajectory equation provided in Eq. (43) with the coefficients given in Eqs. (44), which are based upon the quadratic drag model, requires no special abilities beyond the knowledge and skills gained in a college algebra course, and it can be evaluated without the need for numerical methods.

In a more advanced classroom, Eqs. (38), (39), and (42) could be utilized for a computational project in which students are tasked with determining the projectile location along its trajectory at specified times. This exercise would involve first determining u from Eq. (39) for a particular $\bar{t}$ (e.g., via Newton-Raphson iteration), and then substituting this u into Eqs. (38) in order to evaluate $\bar{x}$ and $\bar{y}$. Of course, this exercise could be entirely accomplished in terms of regular variables (i.e., x, y, and t) by means of Eqs. (8). It also offers an opportunity for exposure to a numerical method that does not require a prior knowledge of how to handle

systems of first-order ODEs (as is needed for implementing Runge-Kutta algorithms to solve such equations).

The author originally developed much of the material presented in this article over a decade ago, but has since updated and refined it during the last several years. It has been utilized to illustrate and demonstrate (at different levels of sophistication) a variety of topics related either directly or indirectly to projectile motion with aerodynamic drag in several undergraduate courses taught on multiple occasions by the author:

- Engineering Orientation – to illustrate proper calculations (with dimensional units)
- Engineering Computation – to demonstrate formulas, macros, and charts in EXCEL®
- Advanced Dynamics – to introduce a problem with a non-linear equation of motion
- Differential Equations – to introduce an application involving a Bernoulli equation
- Engineering Physics – to illustrate aerodynamic drag and dimensionless variables

In each of these courses, the relevant material was well received without apparent difficulties for the students enrolled. The author asserts that the approximate solution advocated herein offers an interesting and instructive approach to presenting a simplified but reasonably accurate model for projectile motion with aerodynamic drag, which hopefully becomes accepted and adopted by engineering and physics educators in the future.

As a final statement concerning the usefulness of the material offered herein, the author wishes to acknowledge that portions of this material are no doubt better suited for upper-division courses or capstone project courses. However, if appropriately adapted and carefully interpreted by an experienced instructor, there are also elements of this material that should prove meaningful and valuable for most students in engineering mechanics and physics courses.

Appendix: A Typical Value for the Parameter α

Most of the results produced by means of the cubic law are fairly accurate if $0 \le \alpha \le 2$. It is then prudent to obtain a typical value of α for a real-world situation involving projectile motion in a resistant medium in order to justify the cubic law and its potential application to other situations. Accordingly, the motion of a baseball through the terrestrial atmosphere after it has been struck by a bat is examined below. Only regular variables (with dimensional units) are considered.

When a solid sphere (representing the baseball) is in motion through a quiescent fluid medium, the magnitude of the drag force F_{d} that acts on the sphere can be modeled [5,6] as

$$F_{\mathrm{d}} = \tfrac{1}{2} C_{\mathrm{d}} A_{\mathrm{c}} \rho_{\mathrm{m}} v^2 \tag{54}$$

The subscripts m and s denote quantities identified with the medium and sphere, respectively; A_{c} is the cross-sectional or profile area of the sphere. Alternatively, Eq. (54) may be recast as

$$F_{\mathrm{d}} = k v^2 \quad ; \quad k \equiv \tfrac{1}{2} C_{\mathrm{d}} A_{\mathrm{c}} \rho_{\mathrm{m}} \tag{55}$$

In addition,

$$\alpha \equiv \sqrt{\frac{k v_{\mathrm{o}}^2}{m g}} \quad , \quad m = \rho_{\mathrm{s}} V_{\mathrm{s}} \quad , \quad \begin{matrix} A_{\mathrm{c}} = \pi r_{\mathrm{s}}^2 \\ V_{\mathrm{s}} = \frac{4}{3} \pi r_{\mathrm{s}}^3 \end{matrix} \tag{56}$$

As a result,

$$\alpha = \sqrt{\frac{3}{8} \frac{\rho_{\mathrm{m}}}{\rho_{\mathrm{s}}} \frac{C_{\mathrm{d}} v_{\mathrm{o}}^2}{r_{\mathrm{s}} g}} \tag{57}$$

The official specifications for a regulation baseball [10] dictate (on average) that

$$r_s = 3.69\,\text{cm} \quad , \quad \rho_s = 691\,\text{kg/m}^3 \tag{58}$$

The fluid medium in this application is standard air, for which

$$\rho_m = 1.20\,\text{kg/m}^3 \quad , \quad \mu_m = 1.81\times10^{-5}\,(\text{N}\cdot\text{s})/\text{m}^2 \tag{59}$$

at a temperature of $293\,\text{K}$ and a pressure of $101.3\,\text{kPa}$. Furthermore, C_d is determined by the *Reynolds number*, a dimensionless group of parameters whose value characterizes the fluid flow conditions in effect (the extent of turbulence and the degree of boundary layer separation). It is denoted by Re and defined by

$$\text{Re} \equiv \frac{\rho_m v_o d_s}{\mu_m} \quad , \quad d_s = 2r_s \tag{60}$$

For this application, $v_o = 44.7\,\text{m/s}$ (i.e., $100\,\text{mph}$) is assumed as a nominal value for the sphere projection speed (i.e., the absolute speed of the baseball as it leaves the bat) [11], in which case

$$\text{Re} = 2.18\times10^5 \quad \Rightarrow \quad C_d = \tfrac{1}{2} \tag{61}$$

as determined by empirical studies for this fluid flow configuration [12]. Thus, Eq. (57) yields

$$\alpha = 1.34 \tag{62}$$

when $g = 9.81\,\text{m/s}^2$. Observe that this value of α lies within the range of acceptability for the approximate results produced by means of the cubic law.

References

[1] G. W. Parker, Projectile Motion with Air Resistance Quadratic in Speed, Amer. J. Phys., Vol. 45, No. 7 (1977), pp. 606–610.

[2] M. A. B. Deakin, G. J. Troup, Approximate Trajectories for Projectile Motion with Air Resistance, Amer. J. Phys., Vol. 66, No. 1 (1998), pp. 34–37.

[3] R. K. Nagle, E. B. Saff, Fundamentals of Differential Equations and Boundary Value Problems, 2nd Edition, Addison-Wesley, Reading, MA, 1996, pp. 73–74.

[4] H. Anton, Calculus with Analytic Geometry, 5th edition, Wiley, New York, 1995, pp. 655–656.

[5] G. K. Batchelor, An Introduction to Fluid Dynamics, Cambridge University Press, London, 1967, pp. 337–343.

[6] J. W. Daily, D. R. F. Harleman, Fluid Dynamics, Addison-Wesley, Reading, MA, 1966, pp. 376–387.

[7] J. C. Hayen, Projectile Motion in a Resistant Medium; Part I: Exact Solution and Properties, Int. J. Non-Linear Mech., Vol. 38, No. 3 (2003), pp. 357–369.

[8] J. C. Hayen, Projectile Motion in a Resistant Medium; Part II: Approximate Solution and Estimates, Int. J. Non-Linear Mech., Vol. 38, No. 3 (2003), pp. 371–380.

[9] H. Anton, Calculus with Analytic Geometry, 5th edition, Wiley, New York, 1995, pp. 844–846.

[10] Office of the Commissioner of Baseball, Official Baseball Rules, Major League Baseball Properties, Inc., New York, 2000 (Section 1.09).

[11] L. L. Zandt, The Dynamical Theory of the Baseball Bat, Amer. J. Phys., Vol. 60, No. 2 (1992), pp. 172–181.

[12] R. H. Sabersky, A. J. Acosta, E. G. Hauptmann, Fluid Flow: a First Course in Fluid Mechanics, 2nd Edition, Macmillan, New York, 1971, pg. 169.

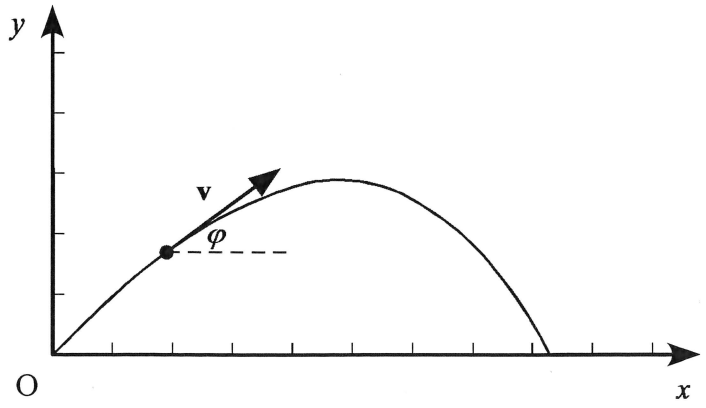

(a)

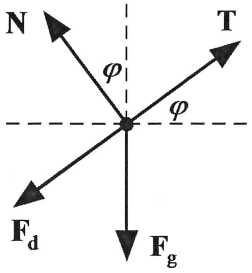

(b)

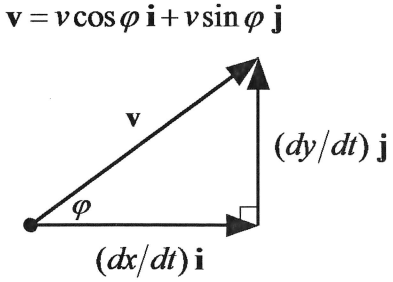

(c)

Figure 1

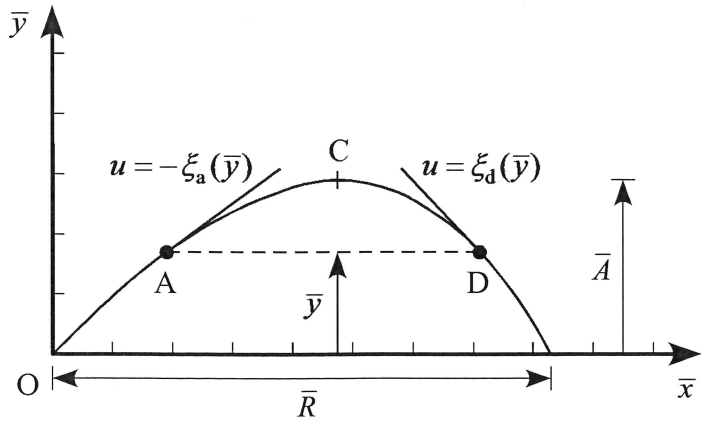

Figure 2

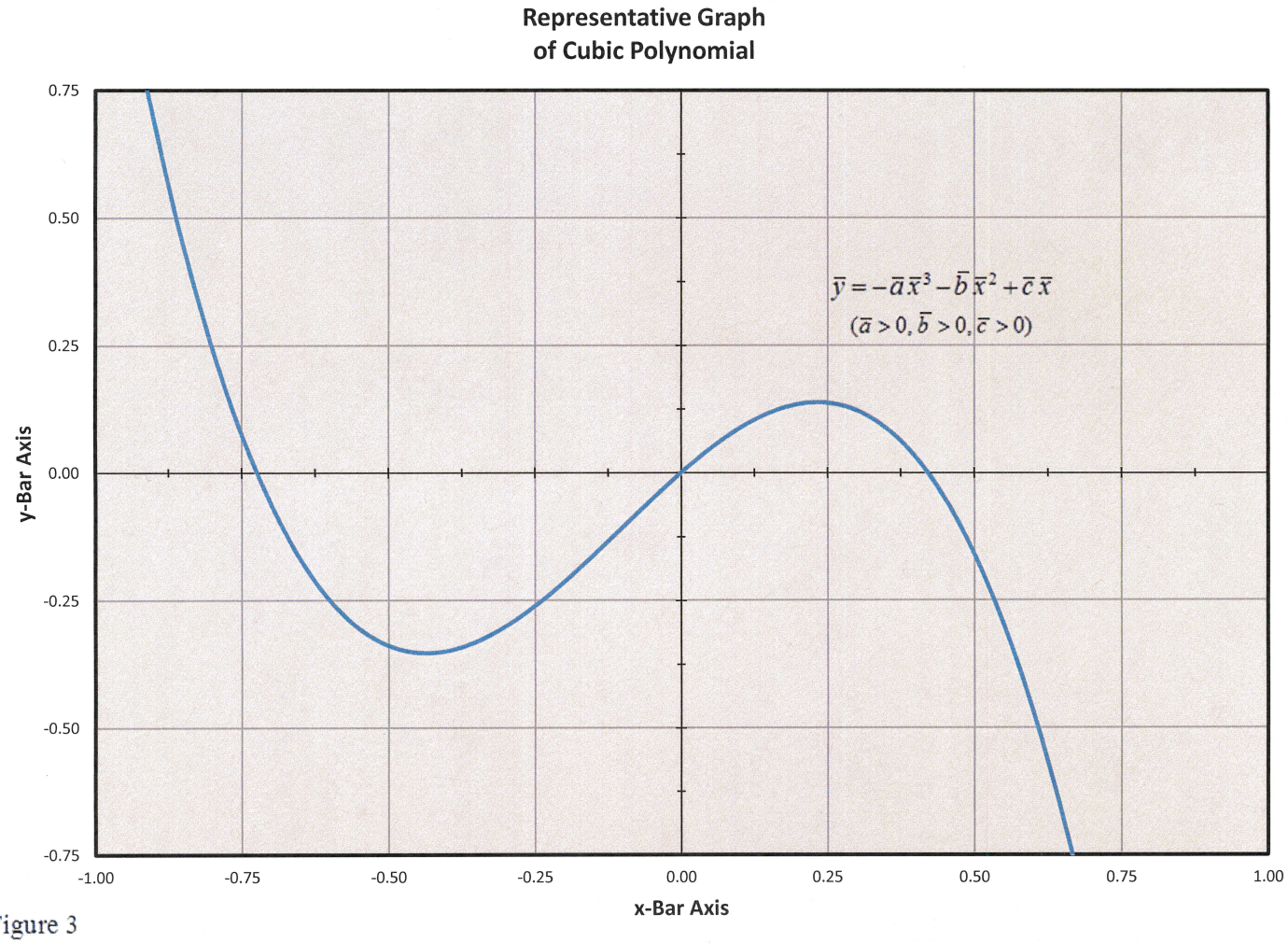
Representative Graph
of Cubic Polynomial
$\bar{y} = -\bar{a}\bar{x}^3 - \bar{b}\bar{x}^2 + \bar{c}\bar{x}$
$(\bar{a} > 0, \bar{b} > 0, \bar{c} > 0)$
y-Bar Axis
x-Bar Axis
0.75
0.50
0.25
0.00
-0.25
-0.50
-0.75
-1.00
-0.75
-0.50
-0.25
0.00
0.25
0.50
0.75
1.00

Figure 3

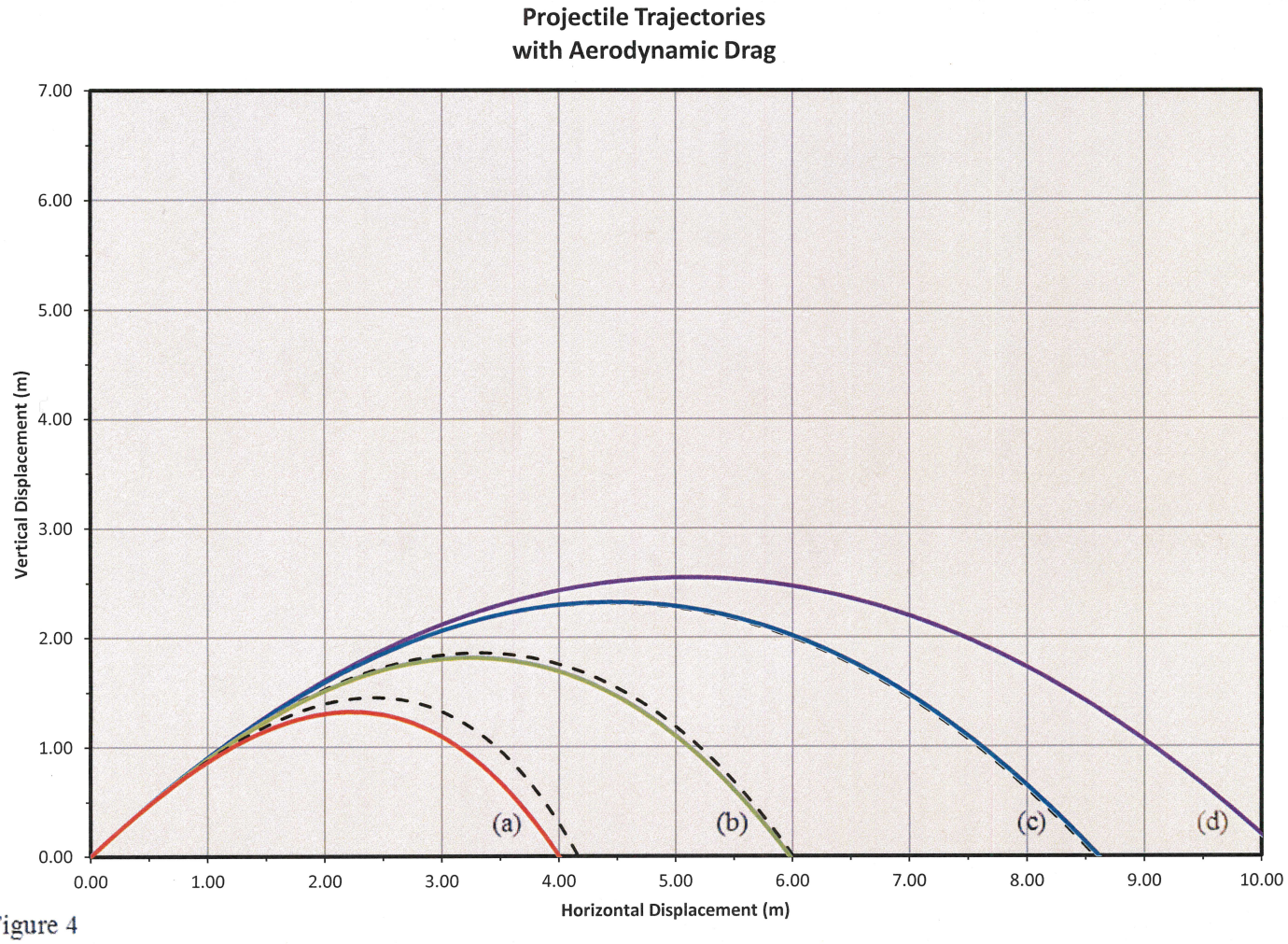
Projectile Trajectories
with Aerodynamic Drag
Vertical Displacement (m)
Horizontal Displacement (m)
7.00
6.00
5.00
4.00
3.00
2.00
1.00
0.00
0.00
1.00
2.00
3.00
4.00
5.00
6.00
7.00
8.00
9.00
10.00
(a)
(b)
(c)
(d)

Figure 4

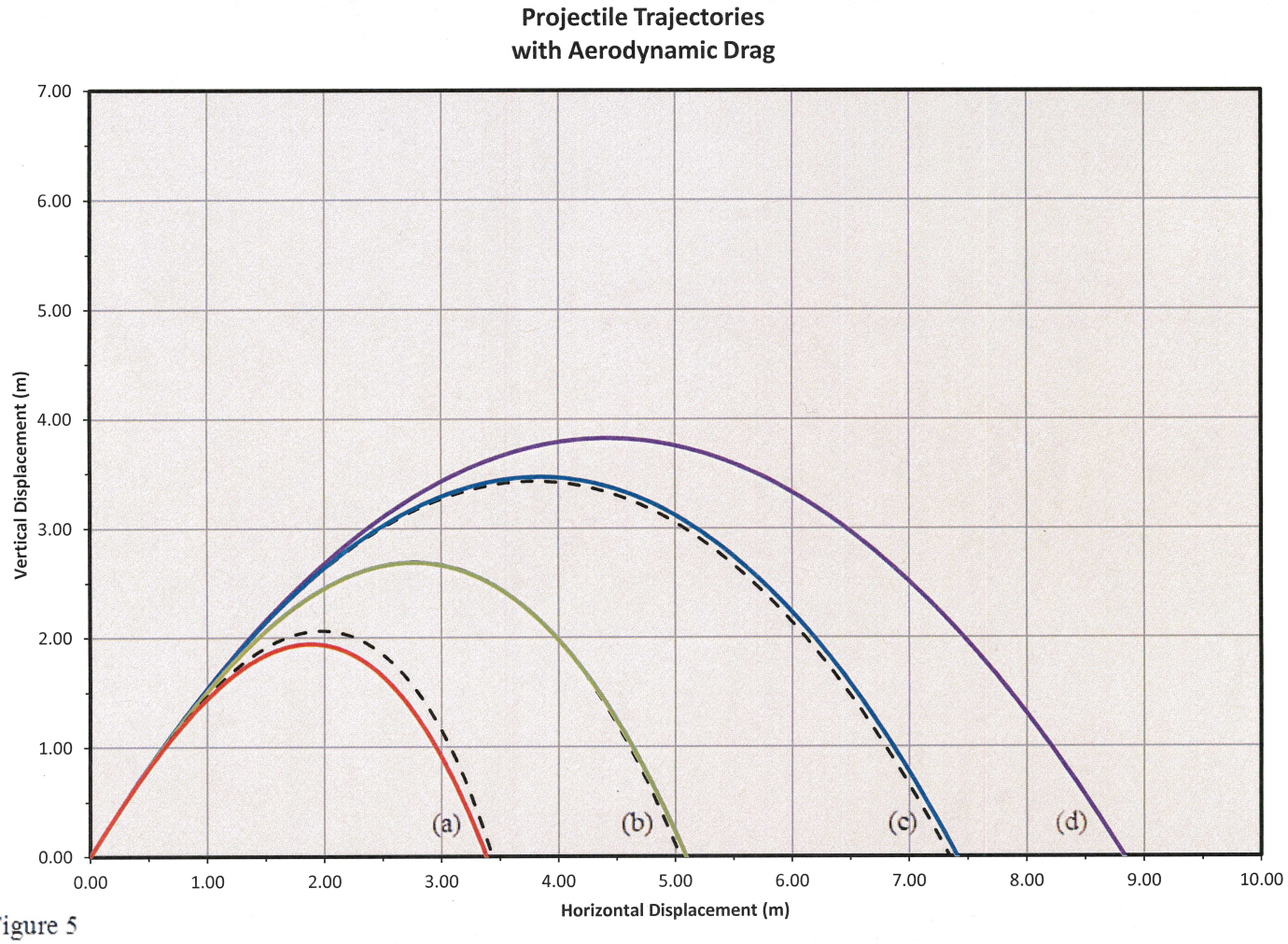
Projectile Trajectories
with Aerodynamic Drag
Vertical Displacement (m)
Horizontal Displacement (m)
7.00
6.00
5.00
4.00
3.00
2.00
1.00
0.00
0.00
1.00
2.00
3.00
4.00
5.00
6.00
7.00
8.00
9.00
10.00
(a)
(b)
(c)
(d)

Figure 5

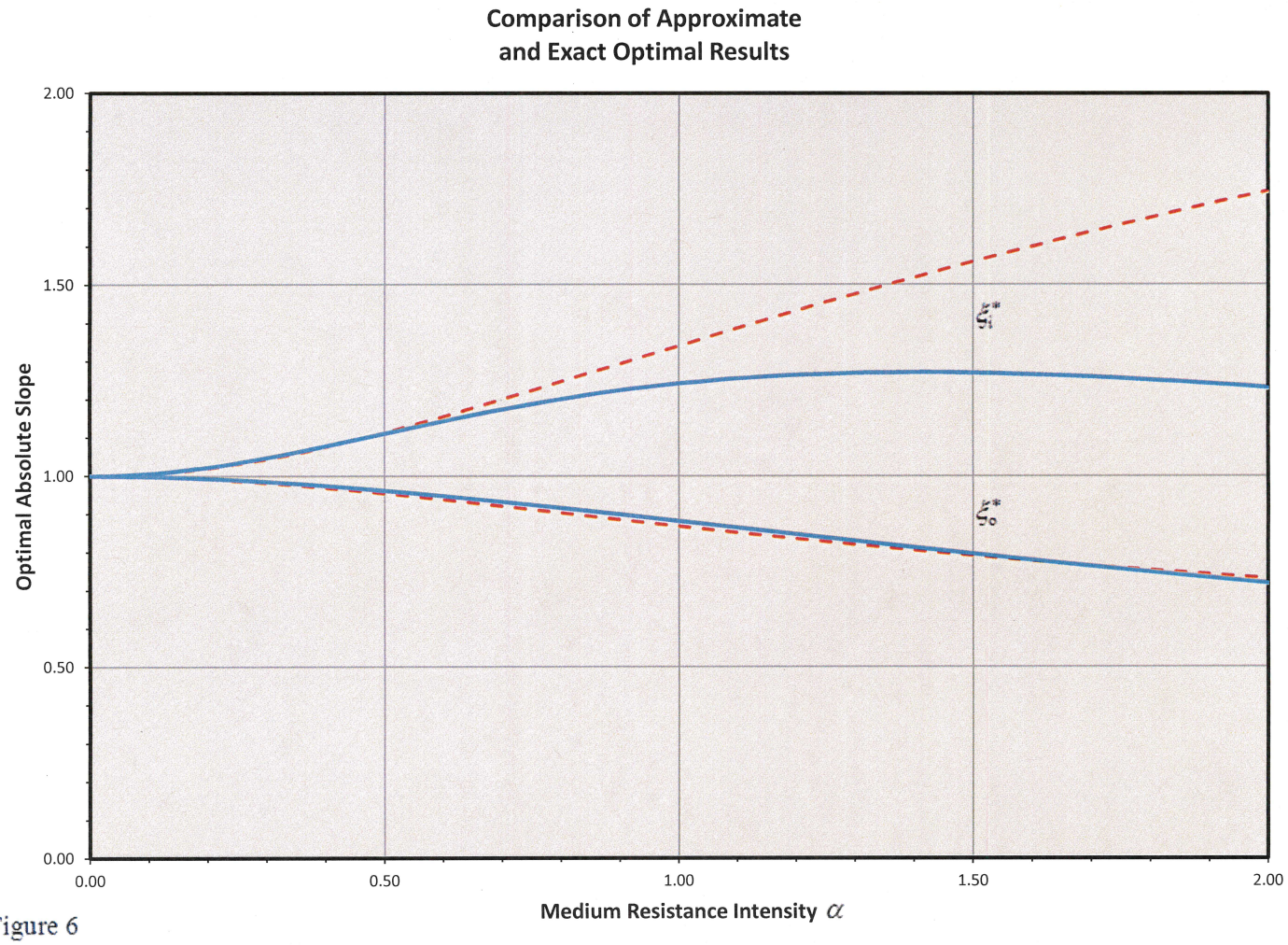
Comparison of Approximate
and Exact Optimal Results
Optimal Absolute Slope
2.00
1.50
1.00
0.50
0.00
0.00
0.50
1.00
1.50
2.00
Medium Resistance Intensity α

Figure 6

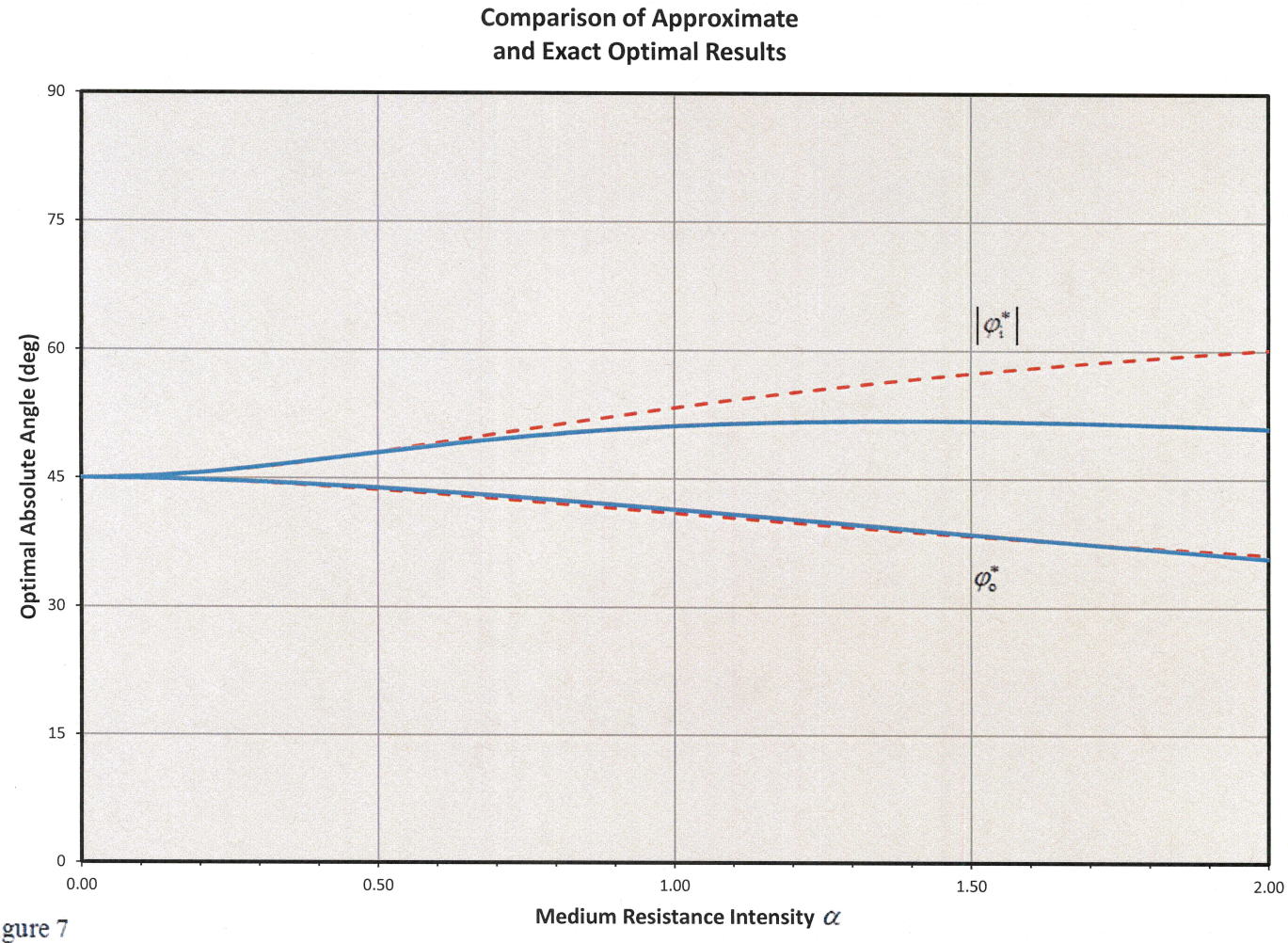
Comparison of Approximate
and Exact Optimal Results
Optimal Absolute Angle (deg)
90
75
60
45
30
15
0
0.00
0.50
1.00
1.50
2.00
Medium Resistance Intensity α
$|\varphi_1^*|$
φ_0^*

Figure 7

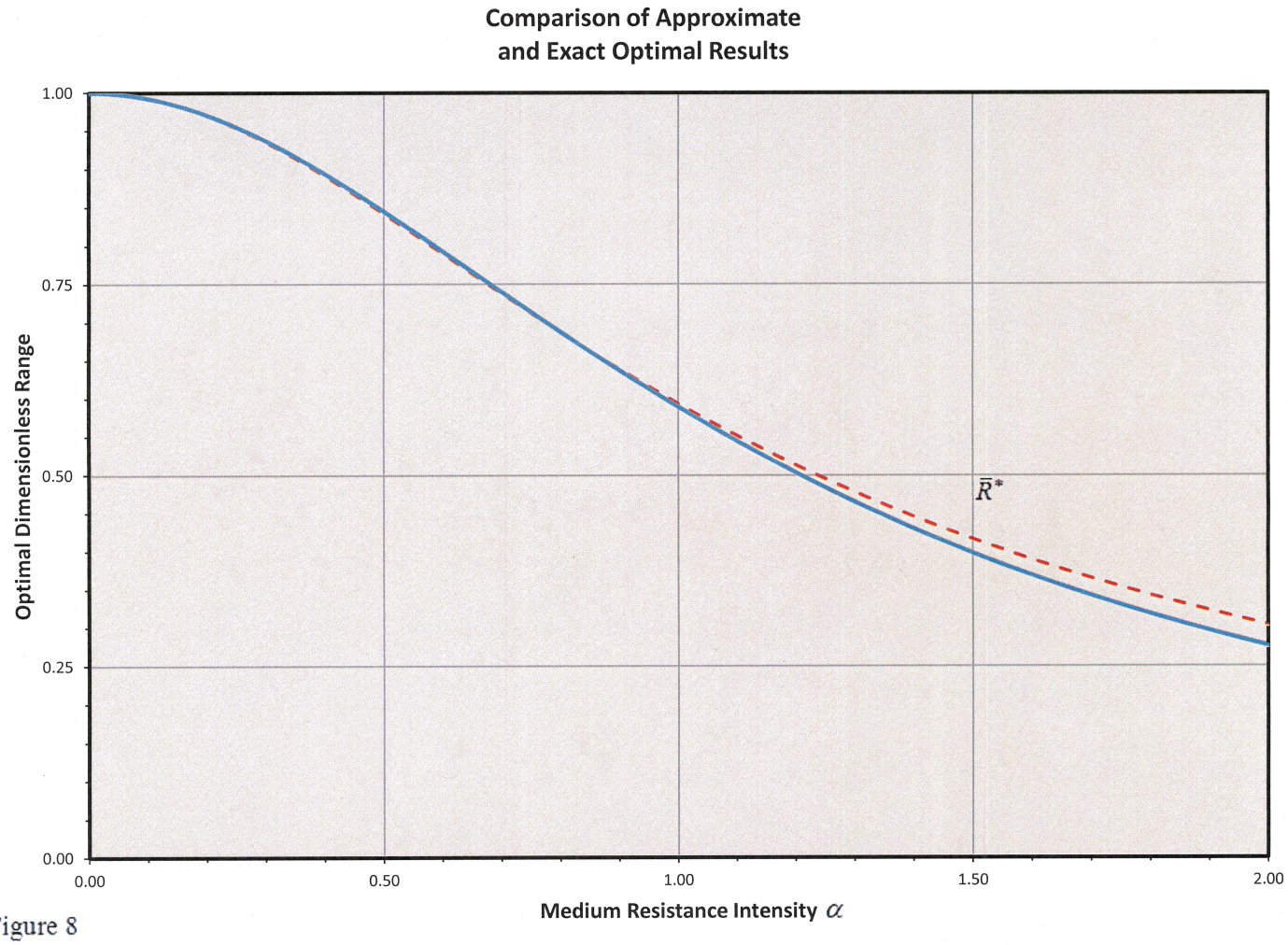
Comparison of Approximate
and Exact Optimal Results
Optimal Dimensionless Range
1.00
0.75
0.50
0.25
0.00
0.00
0.50
1.00
1.50
2.00
Medium Resistance Intensity α
$\bar{R}^*$

Figure 8